The Swapping of Terminal Arms in Ribonucleases: Comparison of the Solution Structure of Monomeric Bovine Seminal and Pancreatic Ribonucleases[†]

Francesca Avitabile,[‡] Caterina Alfano,[‡] Roberta Spadaccini,[‡] Orlando Crescenzi,[‡] Anna M. D'Ursi,[§] Giuseppe D'Alessio,[∥] Teodorico Tancredi,[⊥] and Delia Picone*[,‡]

Dipartimento di Chimica, Università di Napoli "Federico II", Via Cintia, 80126 Napoli, Italy, Dipartimento di Scienze Farmaceutiche, Università di Salerno, 84084 Fisciano, Italy, Dipartimento di Chimica Biologica, Università di Napoli "Federico II", 80134 Napoli, Italy, and Istituto di Chimica Biomolecolare del CNR, via Campi Flegrei 34, 80078 Pozzuoli, Italy

Received February 14, 2003; Revised Manuscript Received May 20, 2003

ABSTRACT: Bovine seminal ribonuclease (BS-RNase), the only dimeric protein among the pancreatic-like ribonucleases, is endowed with special structural features and with biological functions beyond enzymatic activity. In solution, the protein exists as an equilibrium mixture of two forms, with or without exchange (or swapping) of the N-terminal arms. After selective reduction and alkylation of the two intrachain disulfide bridges, the dimeric protein can be transformed into a monomeric derivative that has a ribonuclease activity higher than that of the parent dimeric protein but is devoid of the special biological functions. A detailed investigation of the structural features of this protein in solution, in comparison with those of other monomeric ribonucleases, may help unveil the structural details which induce swapping of the N-terminal arms of BS-RNase. The solution structure of the recombinant monomeric form of BS-RNase, as determined by 3D heteronuclear NMR, shows close similarity with that of bovine pancreatic ribonuclease (RNase A) in all regions characterized by regular elements of secondary structure. However, significant differences are present in the flexible regions, which could account for the different behavior of the two proteins. To characterize in detail these regions, we have measured H/D exchange rate constants, temperature coefficients and heteronuclear NOEs of backbone amides for both RNase A and monomeric BS-RNase. The results indicate a large difference in the backbone flexibility of the hinge peptide segment 16−22 of the two proteins, which could provide the molecular basis to explain the ability of BS-RNase subunits to swap their N-terminal arms.

The investigation of the structural features which control domain swapping, i.e., a process in which two (or more) protomers exchange identical domains, can be useful to understand the mechanisms of assembly of multimeric proteins and their organization as higher order structures (*1*, *2*). It has also been suggested that a similar mechanism controls the formation of amyloidogenic protein aggregates in some misfolding pathologies (*3*−*5*).

The possibility that the two identical subunits of a dimeric protein exchange their terminal arms has been hypothesized in 1962, to explain the recovery of biological activity upon mixing of two inactive forms of bovine pancreatic ribonuclease (RNase A) (*6*). The first X-ray structure of a dimeric protein presenting the exchange of the N-terminal helices between subunits was reported by Mazzarella et al. (*7*). Up to now, about 40 domain-swapped proteins have been identified (*5*).

Recently it has been shown that upon lyophilization from acetic acid, RNase A, the prototype of the tetrapod RNase superfamily, forms different long-lived oligomers, including two types of dimers, two types of trimers, and tetramers and higher oligomers (*8*, *9*). X-ray structures of both dimers revealed that the protomers N-terminal helices are swapped in one dimer (*10*), whereas their C-terminal strands are swapped in the other (*11*). Furthermore, models for trimers and tetramers have been proposed (*12*, *13*), showing that, in a protein, structural elements can be swapped at both N- and C-termini, giving rise to a variety of oligomers.

Dimers, trimers, and other aggregates arise from RNase A only upon treatment in denaturing conditions. None of

[†] Supported by grants from MURST (Prin 2000 and 2002) and CNR (Agenzia 2000).

* Corresponding author. Address: Dipartimento di Chimica, Università degli Studi di Napoli "Federico II", via Cintia 26, Complesso Universitario di Monte S. Angelo, 80126 Napoli, Italy. Phone: +39-081-674406. Fx: +39-081-674409. E-mail: picone@chemistry.unina.it.

[‡] Dipartimento di Chimica, Università di Napoli "Federico II".

[§] Dipartimento di Scienze Farmaceutiche, Università di Salerno.

[∥] Dipartimento di Chimica Biologica, Università di Napoli "Federico II".

[⊥] Istituto di Chimica Biomolecolare del CNR.

[1] Abbreviations: COSY, correlation spectroscopy; HNHA, ^{15}N-separated ^{1}HN−^{1}Hα homonuclear *J* correlated experiment; HNHB, heteronuclear *J* correlated ^{15}N−^{1}Hβ experiment; HSQC, heteronuclear single quantum coherence spectroscopy; IPTG, isopropylthio-β-D-galactoside; NMR, nuclear magnetic resonance; NOE, nuclear Overhauser effect; NOESY, NOE spectroscopy; NOESY-HSQC, ^{15}N edited 3D ^{1}H−^{15}N NOESY; TOCSY, total correlation spectroscopy; TOCSY-HSQC, ^{15}N edited 3D ^{1}H−^{15}N TOCSY; $^{3}J_{HN\alpha}$, vicinal spin−spin coupling constant between the backbone amide proton and the α-proton; $^{3}J_{NH\beta}$, spin−spin coupling constant between the backbone amide nitrogen and one of the β-protons; rmsd, root-mean-square deviation; 2D and 3D, two and three-dimensional; BS-RNase, bovine seminal ribonuclease; mBS, monomeric Asn67Asp BS-RNase with cysteines 31 and 32 linked to glutathione moieties; RNase A, bovine pancreatic ribonuclease.

10.1021/bi0342517 CCC: $25.00
Published on Web 07/04/2003

these structures or models displays similarity with bovine seminal RNase (BS-RNase), the only dimeric member of the tetrapod RNase family (*14*). The two identical subunits of BS-RNase are linked through disulfide bridges between two adjacent cysteines, located at positions 31 and 32. Each subunit is homologous (80% identity) to RNase A. In particular, both enzymes exhibit active sites constituted by identical amino acid residues in the same sequence position. Moreover, BS-RNase is the only known dimeric enzyme characterized, in solution, by an equilibrium between two different structures (*15*): in the form dubbed MxM, the N-terminal arms are swapped between subunits, whereas in the form indicated as M=M, no swapping occurs. In the native protein, the equilibrium ratio between MxM and M=M is 70:30.

Structural details of the MxM form have been obtained by an X-ray diffraction analysis at 1.9 Å resolution (*16)* (PDB entry 1BSR), whereas no data are yet available for the M=M form. As expected on the basis of the high sequence similarity, the secondary structure of each subunit of BS-RNase is very similar to the corresponding one of RNase A. The MxM form presents, however, a marked difference in the region 16−22, with a completely different orientation of the N-terminal peptide, which alters the tertiary structure of the chain and confers a unique feature to the overall structure of the seminal enzyme.

Domain swapping in BS-RNase was reported to be determinant for some special, noncatalytic, biological actions, such as allostery (*17*), cytotoxicity toward malignant cells (*18*, *19*), and immunosuppression and antispermatogenesis (*20*), which may support a physiological role. The active sites of the MxM form are located at the two interfaces between the swapping tails and the main protein bodies and are formed by residues belonging to different chains; in turn, each chain is involved in both active sites.

Folded, stable, and catalytically active monomeric derivatives of BS-RNase can be obtained by selective reduction of the dimeric protein with a moderate excess of dithiothreitol, followed by alkylation of the exposed sulfydryl groups (*21*) or by reaction with glutathione (*22*).

Preliminary NMR studies performed in our labs confirmed that the global fold of this protein is similar to that of all RNase-like proteins of the superfamily (*23*, *24*). The crystal structure, solved very recently at a resolution of 1.45 Å (*25*) shows conclusively that the 3D structure of monomeric BS-RNase is very similar to that of RNase A; furthermore, the folding of the N-terminal arm on its own body gives rise to an active site indistinguishable from that of the MxM form.

Here we report on the solution structure of the Asn67Asp variant of monomeric BS-RNase (mBS) as determined by 3D-heteronuclear NMR. The mutation has been introduced to avoid sample heterogeneity arising from the spontaneous deamidation of Asn^{67} (*26*), which gives rise to a mixture of proteins with Asp or *iso*-Asp at position 67. The comparison of the three-dimensional structure in solution of mBS with that of RNase A, together with the analysis of the backbone flexibility, as determined by heteronuclear NOEs, can be useful to identify the structural basis of the singular features of BS-RNase.

MATERIALS AND METHODS

Escherichia coli strain BL21(DE3) was transformed with a recombinant pET-22b+ plasmid containing cDNA coding either for RNase A or for the Asn67Asp variant of BS-RNase. Unlabeled monomeric BS-RNase, with cysteines 31 and 32 linked to two glutathione molecules, was obtained as described (*24*) with a yield of 15 mg per L of culture. The relative enzymatic activity of the purified mBS with respect to RNase A, as measured by Kunitz assay (*27*) on yeast RNA, was 0.54, in good agreement with the value reported for the native monomer (*28*).

The labeled samples were obtained by growing cells at 37 °C on M9 minimal medium containing 1 g/L of $^{15}NH_4Cl$ up to 0.6 O.D. at 600 nm. Expression was induced by addition of 0.4 mM IPTG. Both proteins were solubilized from inclusion bodies in fully reduced and denaturated form. After renaturation and reoxidation in the presence of the redox couple of oxidized and reduced glutathione (0.6/3 mM), a gel-filtration on G-75 Sephadex yielded 2.5 mg per L of bacterial medium of mBS or 3 mg/L of RNase A.

NMR Spectroscopy. NMR measurements on 2 mM samples of proteins dissolved in 95% H_2O−5% D_2O at pH 5.65 and 300 K were performed on Bruker DRX400, DRX500 and DRX600 spectrometers, using 5 mm small volume NMR sample tubes (NewEra). Data processing was performed with NMRPipe (*29*) and spectral analysis with NMRView (*30*). ^1H chemical shifts are relative to the water signal at 4.70 ppm at 300 K. ^{15}N chemical shifts were indirectly referenced to the ^1H chemical shifts according to magnetogiric ratios (*31*).

The assignment of proton and ^{15}N resonances of mBS has been reported elsewhere (*24*) (BioMagResBank entry 4980): 122 spin systems, out of 125 residues (taking into account the N-terminal Met^0), were partially or completely assigned. Unassigned backbone resonances correspond to Met^0, Lys^1, and Phe^{120}. The HN resonance of Phe^{120} is absent in the NMR spectra acquired at 300 K but was detected by lowering the temperature to 277 K.

The backbone assignment of RNase A in the same experimental conditions was achieved by a combination of 2D and 3D experiments collected at 500 MHz, 300 K.

The heteronuclear-edited 3D experiments used in the assignment procedure were $^1H-^{15}N$ NOESY-HSQC (*32*) and $^1H-^{15}N$ TOCSY-HSQC (*33*). Data size was typically 150 × 32 × 512 complex points in the t_1, t_2, and t_3 time domains, which was zero-filled to obtain 300 × 128 × 1024 data points in the spectrum.

$^3J_{HNH\alpha}$ coupling constants were measured by means of 3D HNHA, a $^1H^{15}N-^1H_\alpha$ correlation experiment (*34*). $^3J_{NH\beta}$ coupling constants were measured by means of 3D HNHB, a $^{15}N-^1H\beta$ correlation experiment (*35*). Data size was 64 × 47 × 512 complex points, which was zero-filled to obtain 128 × 94 × 1024 data points for the HNHA spectrum, and 80 × 32 × 512 complex points, which was zero-filled to obtain 160 × 64 × 1024 data points for the HNHB.

Series of decoupled HSQC experiments (*36*) were used to identify amide protons with slowed exchange, after dissolving a freeze-dried protein sample in 99.9% D_2O. Amide proton temperature coefficients were also measured from HSQC spectra in the temperature range 277−315 K for mBS and 285−310 K for RNase A.

Heteronuclear {^{1}H}−^{15}N NOEs were measured at 500 MHz using the 2D pulse sequences published by Farrow et al. (*37*), whereby the ^{1}H-presaturated and reference experiments were collected in the interleaved mode.

Proline Isomerism. On the basis of $H_\alpha-H_\alpha$ (i,i+1) and $HN-H_\alpha$ (i,i+1) NOEs, we assigned *cis* isomerism to proline residues 93 and 114, whereas trans isomerism was observed for Pro^{117} and Pro^{42}, on the basis of $H_\alpha-H_\delta$ (i,i+1) and $HN-H_\delta$ (i,i+1) NOEs, consistent with the findings for RNase A (*38*, *39*) and BS-RNase (*7*, *40*). Pro^{19}, which is not present in RNase A, was also assigned a trans configuration on the basis of a NOE between Ser^{18} H_α and Pro^{19} H_δ. The presence of a sizable population of the cis isomer cannot, however, be excluded, since the resonances of Ser^{18} H_α and Pro^{19} H_α are too close for a conclusive detection of diagnostic NOEs.

Collection of Structural Restraints and Calculation of the Three-Dimensional Structure. Interproton distances were derived from cross-peak integrals on a ^{15}N edited 3D ^{1}H−^{15}N NOESY-HSQC (*32*) in H_2O and on 2D NOESY both in H_2O and in D_2O, all acquired with 80 ms mixing time. Peak integrals were evaluated with the program NMRView (*30*), transferred to the program package DYANA 1.5 (*41*), and converted into upper distance limits by using CALIBA (*42*). Spin coupling values were input into HABAS (*43*) to obtain the possible ranges of torsion angles with simultaneous consideration of the NOE-derived distance restraints. During all the steps, the four histidine side chains were considered in the protonated state, according to their pK_a values in RNase A (*44*). Several rounds of calculations were iterated starting from the initially obtained solid NOE assignments to extend the assignments of the NOE peaks, using as filter in the NMRView analysis the preliminary bundle of structures determined in the previous calculation step. Typical DYANA runs were performed on 200 randomly generated starting structures with 10 000 torsion angle dynamics steps. A total of 2281 NOESY cross-peaks was determined, and after selection of redundancies and inconsistencies with the aid of CALIBA, 1275 distance, 43 hydrogen bond, and 314 dihedral angle restraints were incorporated in the final calculation. In the refinement step, these distance and angle restraints were converted into the input format used in AMBER (*45*). The 80 DYANA structures with the lowest target function values were subjected to restrained energy minimization using the sander_classic module of AMBER 6.0 (*45*). The 1991 version of the all-atom force field was used (*46*), with a distance-dependent dielectric constant $\epsilon = r_{ij}$. To reduce the artifacts that can arise during in vacuo simulation, the charge of the ionizable groups was reduced to 20% of its full value. No distance cutoff was used in the evaluation of nonbonded interactions. Distance restraints were applied as a flat well with a parabolic penalty within 0.5 Å outside the upper bound and a linear function beyond 0.5 Å, using a force constant of 16 kcal mol^{-1} Å^{-2}, whereas a force constant of 16 kcal mol^{-1} rad^{-2} was used for angle restraints. No hydrogen bond restraints were used during this phase of the refinement. The restrained energy minimization was carried out with a total of 10 000 steps of steepest descent/conjugated gradient minimization for each conformer. The best 16 structures, among those with a total energy lower than −1306 kcal mol^{-1}, were selected to represent the solution structure.

Exchange Rates and Temperature Coefficients of Amide Protons. Exchange rates of amide protons were determined by recording aseries of ^{1}H−^{15}N HSQC spectra at different times, beginning immediately after dissolving a freeze-dried protein sample in D_2O. For the aim of structure calculation, amide protons were classified on the basis of exchange data into three categories: fast-exchange (signals virtually disappeared within thirty minutes), slow exchange (signals still visible after two hours), and very slow exchange (signals still visible after 12 h). To complement this information, we measured also HN temperature coefficients over a wide temperature range. Series of ^{1}H−^{15}N HSQC spectra on 200 μM samples yielded temperature coefficients for most amide chemical shifts. According to Baxter and Williamson (*47*), when an amide proton exchanges slowly and has a temperature coefficient more positive than −4.5 ppb/K, it is hydrogen bonded. Exchange and temperature data show indeed significant consistency and allowed the identification of 46 protons potentially involved in hydrogen bonds. To use this information in the structure calculation, we selected only protons that, in addition to the exchange and temperature coefficient criteria, showed clear NOE patterns characteristic of secondary structures. For the 43 hydrogen bonds thus identified, the NH−O distance was restrained to 2.0 Å, and the N−O distance was kept at 3.0 Å in DYANA runs. Hydrogen bonds were not restrained in the AMBER minimizations.

Computations were performed on SGI O2 and Linux workstations.

Display of the structures and calculations of the mean structure and of root-mean-square deviations relative to the mean were carried out with the program MOLMOL (*48*) or MolScript (*49*).

Diffusion Measurements. Diffusion measurements were carried out at 300 K and 500 MHz on two matched samples of unlabeled mBS and of RNase A (Sigma, type XII-a) containing 1.3 mM solutions of protein in H_2O, 5% D_2O at pH 5.65; small volume tubes (14 mm sample height) were used in order to confine the samples within the linear region of the gradient coils. Gradient strengths were calibrated by the method which involves recording the spectrum of a phantom in water (*50*, *51*), and were checked by measuring the diffusion coefficient of a D_2O sample (at 298 K, using the reference values reported in ref. *51*), with comparable results (63 G/cm at 100% strength). A longitudinal eddy current delay pulse sequence incorporating bipolar square gradient pulses was used (*52*), and for each of the two protein samples, 18 diffusion-attenuated 1D spectra (including three duplicates) were recorded, at different gradient strengths; the aliphatic region of the spectrum was integrated, and the values were fitted to an exponential decay function, as described in refs *50* and *51*. The ratio of the diffusion coefficients of mBS to RNase A was 0.962 ± 0.014: the slight deviation from unity can in part be accounted for by the presence in mBS of Met^0 and two glutathione units, which are missing in commercial RNase A.

RESULTS

The NMR Solution Structure of mBS. The solution structure of mBS, similar to those of other mammalian ribonucleases and of angiogenin, has the shape of a kidney. It can be

Table 1: Structural Statistics

quantity	16 conformers
Residual Distance Constraint Violations[a] (Å)	
$0.1 < d \leq 0.2$	35.4 ± 4.7
$0.2 < d \leq 0.3$	9.0 ± 2.1
$0.3 < d \leq 0.4$	1.2 ± 0.9
$0.4 < d \leq 0.5$	0.4 ± 0.5
$0.5 < d$	0
maximum violation	0.38 ± 0.07
Residual Dihedral Angle Constraint Violations[a] (deg)	
$0 < \vartheta \leq 5$	26.6 ± 4.9
$5 < \vartheta \leq 10$	4.3 ± 1.6
$10 < \vartheta \leq 20$	2.5 ± 1.0
$20 < \vartheta$	0
maximum violation	14.6 ± 2.5
AMBER Energies (kcal mol^{-1})	
distance constraints	27.2 ± 3.2
torsional constraints	4.1 ± 1.1
van der Waals	-658.9 ± 10.8
total	-1346.2 ± 30.9
rmsd to the Averaged Coordinates[b] (Å)	
backbone (secondary structure)[c]	0.760
all heavy (secondary structure)[c]	1.317
Structure Quality by PROCHECK Analysis (*53*)	
residues in most favored regions	72.4%
residues in additional allowed regions	23.9%
residues in generously allowed regions	2.5%
residues in disallowed regions	1.2%

[a] Average value for the 16 energy minimized conformers. [b] Average coordinates of the 16 energy minimized conformers after best fit superposition of the backbone atoms of residues 5−12, 23−33, 43−47, 51−58, 61−64, 71−74, 79−86, 97−104, 106−110, and 117−123. [c] Residues 43−47, 61−64, 71−74, 79−86, 97−104, 106−110, and 117−123 correspond to the main β strands, while residues 5−12, 23−33, and 51−58 correspond to the α-helices.

described as two antiparallel β-sheets, which form a characteristic V-shaped motif, and three short α-helices. In the mean structure, one of the β-sheets is constituted by residues 61−64, 71−74, 106−110, and 117−123, the other one by residues 43−47, 79−86, and 97−104; the three helices span residues 5−12, 23−33 and 51−58.

The satisfactory quality of the structure determination (13 constraints/residue) is reflected by the global rmsd value (0.76 Å) relative to the mean coordinates for the backbone atoms, referred to parts of the structure that are not intrinsically flexible. Table 1 summarizes the relevant statistics of the structure determination procedure.

Figure 1 shows a view of the final bundle of structures: rmsds from the average are 0.76Å (backbone heavy atoms) and 1.32 Å (all heavy atoms) for all residues in regular secondary structure regions.

The intrinsic flexibility of the remaining regions, in particular of the hinge peptide spanning residues 16−22, is reflected by the number and type of NOE constraints, as can be seen in Figure 2, which shows the distribution of distance constraints as a function of the residue number.

The quality of the ensemble of structures was checked with PROCHECK (*53*): the ϕ and ψ angles of 72.4% of all residues fall in most favored regions, 23.9% in additional allowed regions, 2.5% in generously allowed regions, and 1.2% in disallowed regions of the Ramachandran−Sasisekharan plot (*54*). Figure 3A shows the superposition of the mean structure of mBS with that of RNase A, derived from the NMR bundle (*38*) (PDB entry 2AAS). The rmsd calculated over the elements of secondary structure common to both proteins is 1.26 Å, thus confirming a high similarity between their solution structures. Some differences are present in the second helix, which in RNase A is shorter by two residues, starting at Tyr^{25} instead of Ser^{23}, and in the region 61−64, which is a regular β-strand in RNase A but is less ordered in mBS. However, the most relevant differences are in the flexible regions. In particular, several hydrogen bonds involving backbone atoms as well as side-chains are present in the 16−22 hinge region of RNase A (NH's of Asp^{14}, Ser^{16} and Ala^{20} to the CO of Val^{47} and the side-chain oxygens of Asp^{14} and Gln^{101}, respectively), whereas in the corresponding region of mBS, only two hydrogen bonds (NH of Asp^{14} to the CO of Val^{47} and NH of Ser^{20} to the CO of Ser^{18}) are present in about half of the structures. The loop spanning residues 65−72, which in the native enzyme is involved in the deamidation of Asn^{67}, is one of the most disordered regions of mBS, whereas it is rather well defined in RNase A. By contrast, the region 112−115, which is central to the swapping of the C-terminal arms in RNase A dimers, shows no relevant structural differences despite the high number of sequence substitutions.

Comparison Between the Dynamic Properties of RNase A and mBS. To allow a more detailed comparison between RNase A and mBS, we resorted to experimental measurements directly related to the dynamic properties of the proteins in solution, i.e., H/D exchange rates, temperature coefficients of amide protons, and $\{^1H\}-^{15}N$ heteronuclear

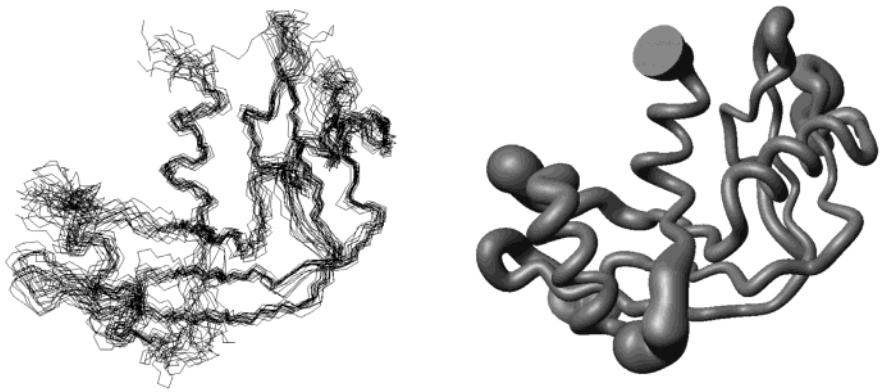

FIGURE 1: Bundle of the best 16 structures of mBS after AMBER minimization, superimposed for backbone atoms of residues 5−12, 23−33, 43−47, 51−58, 61−64, 71−74, 79−86, 97−104, 106−110, and 117−123 (left side) and corresponding mean structure (right side).

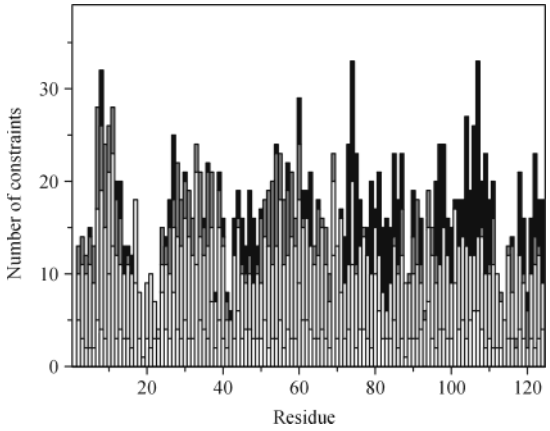

FIGURE 2: Distribution of the NOE constraints as a function of the residue number. White bars, intraresidue effects; light gray, sequential; gray, medium range; black, long range.

NOEs. As a first step of this analysis, we assigned the backbone resonances of both proteins at the same pH and temperature conditions. A ^{15}N-labeled sample of RNase A was prepared as described in the Experimental Section. Figure 3B shows the superposition of HSQC spectra of RNase A and mBS at 300 K, pH 5.65. We analyzed a new set of 3D experiments (^{1}H−^{15}N TOCSY-HSQC and ^{1}H−^{15}N NOESY-HSQC) using the literature data available in BioMagResBank (entry code 4032) (*55*) as a starting point. Exchange rate constants of amide protons for both proteins were estimated by measuring the intensities of cross-peaks in a series of ^{1}H−^{15}N HSQC spectra at different times, starting within 20′ from the dissolution of the freeze-dried protein in D_2O. The intensities were fitted to an exponential function $I(t) = I_0e^{-kt}$. Amide protons were classified on the basis of exchange data into three categories: fast-exchanging ($k_{exch} \geq 9$ h^{-1}), medium-exchanging ($k_{exch} = 7-9$ h^{-1}), and slow-exchanging ($k_{exch} < 7$ h^{-1}). Temperature coefficients were measured by a series of ^{1}H−^{15}N HSQC spectra at different temperatures in a wide temperature range. The k_{exch} of the slow exchanging amide protons and the temperature coefficients measured for mBS and RNase A are reported as Supporting Information. Figure 4 shows a ribbon representation of the two proteins, color-coded according to the temperature coefficients of amide protons.

Exchange and temperature data show substantial consistency when comparing conserved residues which are also involved in regular secondary structure elements, such as, for instance, residues 5−12 of the N-terminal helix. The only significant exception is represented by the residues of the second helix, where all the amide protons of the residues from 28 to 34 are characterized by slow exchange and low temperature coefficients in mBS, whereas in RNase A, residues 26, 27, and 28 are fast-exchanging. However some differences are expected not only for the substitution in BS-RNase of Cys^{31}, Cys^{32}, and Lys^{34} for Lys^{31}, Ser^{32}, and Asn^{34} of RNase A, but also for the presence in mBS of two glutathione moieties, which could limit the solvent accessibility of this region in mBS. Moreover, a good correspondence between the two proteins can also be found for most of residues with outstanding values of temperature coefficients and fast H/D exchange rate (Ser^{50}, Gly^{88}, Tyr^{92}, and Thr^{99}).

However, the main goal of these measurements was to obtain information on the flexible regions, and mainly on those which seem responsible for some differences between RNase A and BS-RNase: the hinge loop (16−22), which controls the swapping of N-terminal ends; the loop 65−72, related to the deamidation of Asn^{67} which occurs spontaneously in wild-type BS-RNase; and the loop centered on Pro^{114}, involved in the swapping of C-terminal ends in some of the RNase A oligomers.

For the 16−22 hinge region, we observe that in RNase A the amide protons of residues Thr^{17}, Ala^{19}, and Ser^{22} have a small negative temperature coefficient, compatible with the presence of hydrogen bonds, whereas in mBS all residues

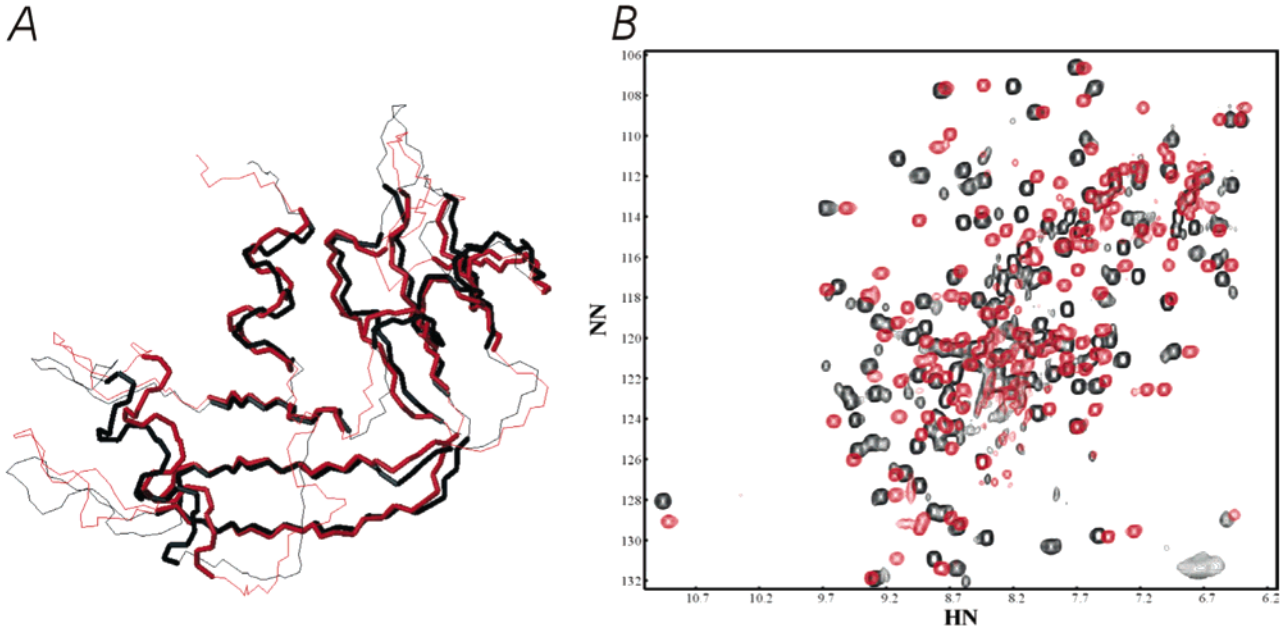

FIGURE 3: (A) Superposition between the NMR mean structures of mBS (black) and RNase A (red, PDB entry 2AAS). The rmsd calculated by fitting the regions with regular elements of secondary structure common to both proteins (residues 5−12, 24−33, 43−47, 51−58, 61−64, 71−74, 79−86, 97−104, 106−110, and 117−123, thick lines) is 1.26 Å. (B) Comparison of the ^{1}H−^{15}N HSQC spectra of mBS (black contour peaks) and RNase A (red contour peaks) at pH 5.65, 300 K.

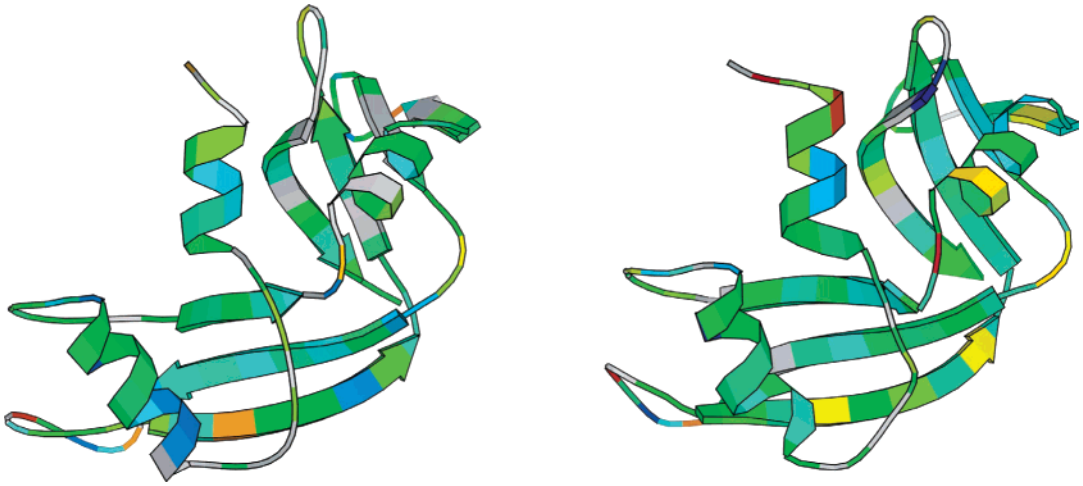

FIGURE 4: Ribbon representation of mBS (left side) and RNase A (right side). The different colors reflect the temperature coefficients of amide protons, ranging from blue (+1.5 ppb/K) to red (−11.5 ppb/K). Grey corresponds to not determined values.

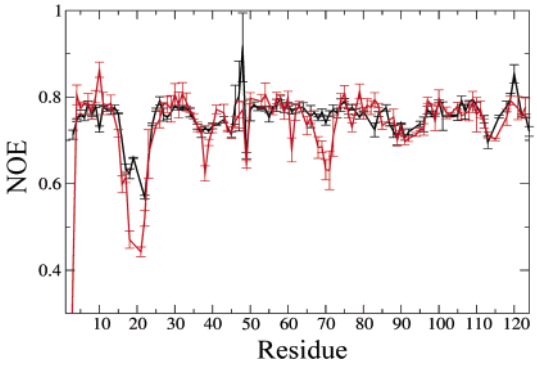

FIGURE 5: Heteronuclear $\{^1H\}-^{15}N$-NOEs of mBS (red) and RNase A (black) at pH 5.65, 300 K.

in this region are completely exposed to the solvent. It should be mentioned that in the NMR structure of RNase A Thr^{17} NH is hydrogen bonded to Asp^{14} CO. Interesting differences are observed also for the loop 65−72, where, despite the high similarity in the amino acid sequence, NHs of both Asp^{67} and Gly^{68} seem hydrogen-bonded (slow exchange, temperature coefficient ≥ 4.5 ppb/K) in mBS but not in RNase A; Gln^{69} is slow-exchanging, and Lys^{66}, Thr^{70}, and Asn^{71} have a low temperature coefficient. In contrast, in RNase A the only residues in this region exhibiting nonrandom temperature coefficient values are Gly^{68} and Asn^{71}.

A more significant comparison of the backbone flexibility between the two proteins has been perfomed by measuring $\{^1H\}-^{15}N$ heteronuclear NOEs (Figure 5). Again, the pattern for mBS nd RNase A is very similar when regions with regular secondary structure are compared, but some relevant differences are present in the loop regions. In particular, the hinge peptide 16−22 is the most flexible region in both proteins, but the heteronuclear NOE pattern indicates very clearly that the mobility for mBS is much higher than for RNase A. The loop 65−72 of mBS is also endowed with a flexibility higher than in RNase A, whereas no differences are present in the loop region centered on Pro^{114}.

DISCUSSION

RNase A and mBS share 101 out of 124 residues (102 out of 125 if we consider Met^0 in the recombinant samples) and are phylogenetically related. Despite this homology, they are endowed with different structural and functional properties such as, for instance, with respect to the swapping of N- and C-terminal tails in their dimeric counterparts. The first peculiarity of the seminal protein is the presence of two cysteine residues at positions 31 and 32: as a consequence, native BS-RNase is a dimer. However, it has been shown that, when the two cysteines are introduced in RNase A, the mutant protein becomes a dimer but does not undergo swapping and is devoid of any special biological activity (*56*), thus suggesting that other residues are also responsible of the structural differences between the two ribonucleases. As already pointed out, the aim of this work is to compare in detail the solution structures of the two monomeric proteins in order to understand the different behavior of the dimers with respect to domain swapping. The NMR solution structure of RNase A at pH 4.0 and 308 K has been published by Santoro et al. (*38*), and very recently a relaxation study at pH 6.4 and 298 K has been reported by Cole and Loria (*57*).

As a first step of this work, we solved the solution structure of mBS by heteronuclear 3D NMR. The distribution of distance constraints along the sequence (Figure 2), in comparison with the plot of the heteronuclear NOEs for the backbone amides (Figure 5), shows that the regions with a low number of constraints are the highly flexible ones. The mBS solution structure is very similar to the subunit of the MxM form of BS-RNase in the crystal structure (apart from the obvious differences in the hinge regions) and to both the crystal and solution structures of RNase A. Some differences are located in the regions of regular secondary structure: in particular, helix 2 (residues 25−32) is rather well defined but assumes slightly different orientations in the different structures of the NMR bundle. This dislocation could be connected to the high flexibility of the contiguous 16−22 segment. An anomalous behavior of this helix has been evidenced also in the temperature coefficients and H/D exchange rates. However, as already pointed out, it should be considered that mBS has two glutathione moieties bound to cysteines 31 and 32, which could induce some discrepancies between the structures.

Another region less regular in mBS than in RNase A is the 61−64 strand, which in some structures of our bundle is shorter (starting at residue 62 or ending at residue 63) or

even absent. The distortion of this region might be related to the substitution of Ala^{64} in RNase A with threonine in mBS and could in turn also increase the mobility of the 65−72 loop, where no differences in primary structure are present. Moreover, the increased flexibility of this region in solution can be related to the observation that in the X-ray structure of native dimeric BS-RNase, the 65−72 loop adopts two different conformations (*16*). It is also possible that the Asn67Asp mutation disturbs the formation of the unusual C_{10} loop present in RNase A, where the side-chain oxygen of Asn^{67} is involved in a hydrogen bond with the amide proton of Gln^{69}.

Heteronuclear $\{^1H\}-^{15}N$-NOEs show only a limited number of differences. Moreover, all of them evidence an increased flexibility of mBS with respect to RNase A, and in general they correspond to regions where residue substitution occurs, as in the case of the hinge 16−22, which in mBS has a very high flexibility. Interestingly, the loop centered around Pro^{114} has a very similar flexibility despite the high number of substitutions (3 out of 5 residues), thus suggesting that the different behavior of the two proteins with respect to the swapping of the C-terminal end is not controlled by backbone mobility on picosecond/nanosecond time scale. Site-directed mutagenesis experiments are in progress to assess these findings.

ACKNOWLEDGMENT

We thank the CIMCF of the University "Federico II" of Naples, where we acquired part of the NMR spectra, Professor Alberto Di Donato for hospitality and advice in the preparation of protein samples, and Professor Lelio Mazzarella for critical reading. Special thanks to Professor Piero A. Temussi for constant encouragement and critical reading. We are also grateful to Dr.Carmine Ercole for assistence with protein expression and to Dr. Maria Rosaria Naddeo for performing the enzymatic assays.

SUPPORTING INFORMATION AVAILABLE

Lists of H/D exchange rate constants and temperature coefficients of amide protons are available. The coordinates have been deposited in the Protein Data Bank under access code 1O0G. This material is available free of charge via the Internet at http://pubs.acs.org.

REFERENCES

1. Bennett, M. J., Schlunegger, M. P., and Eisenberg, D. (1995) *Protein Sci. 4*, 2455−2468.
2. Schlunegger, M. P., Bennett, M. J., and Eisenberg, D. (1997) *Adv. Protein Chem. 50*, 61−122.
3. Klafki, H. W., Pick, A. I., Pardowitz, I., Cole, T., Awni, L. A., Barnikol, H. U., Mayer, F., Kratzin, H. D., and Hilschmann, N. (1993) *Biol. Chem. Hoppe Seyler 374*, 1117−1122.
4. Prusiner, S. B. (1998) *Adv. Virus Res. 35*, 83−136.
5. Liu, Y., and Eisenberg, D. (2002) *Protein Sci. 11*, 1285−1299.
6. Crestfield, A. M., Stein, W. H., and Moore, S. (1962) *Arch. Biochem. Biophys. 1*, 217−222.
7. Mazzarella, L., Mattia, C. A., Capasso, S., and Di Lorenzo, G. (1987) *Gazz. Chim. Ital. 117*, 91−97.
8. Libonati, M., Bertoldi, M., and Sorrentino, S. (1996) *Biochem. J. 318*, 287−290.
9. Gotte, G., Bertoldi, M., and Libonati, M. (1999) *Eur. J. Biochem. 265*, 680−687.
10. Liu, Y., Hart, P. J., Schlunegger, M. P., and Eisenberg, D. (1998) *Proc. Natl. Acad. Sci. U.S.A. 95*, 3437−3442.
11. Liu, Y., Gotte, G., Libonati, M., and Eisenberg, D. (2001) *Nat. Struct. Biol. 8*, 211−214.
12. Adinolfi, S., Piccoli, R., Sica, F., and Mazzarella, L. (1996) *FEBS Lett. 398*, 326−332.
13. Nenci A., Gotte G., Bertoldi M., and Libonati, M. (2001) *Protein Sci. 10*, 2017−2027.
14. D'Alessio, G., Di Donato, A., Mazzarella, L., and Piccoli, R. (1997) in *Ribonucleases: Structures and Functions* (D'Alessio, G., Riordan, J. F., Eds.) pp 383−423, Academic Press, New York.
15. Piccoli, R., Tamburrini, M., Piccialli, G., Di Donato, A., Parente, A., and D'Alessio, G. (1992) *Proc. Natl. Acad. Sci. U.S.A. 89*, 1870−1874.
16. Mazzarella, L., Capasso, S., Demasi, D., Di Lorenzo, G., Mattia, C. A., and Zagari, A. (1993) *Acta Crystallogr. D49*, 389−402.
17. Piccoli, R., Di Donato, A., and D'Alessio, G. (1988) *Biochem. J. 253*, 329−336.
18. Cafaro, V., De Lorenzo, C., Piccoli, R., Bracale, A., Mastronicola, M. R., Di Donato, A., and D'Alessio, G. (1995) *FEBS Lett. 359*, 31−34.
19. Russo, A., Antignani, A., Giancola, C., and D'Alessio, G. (2002) *J. Biol. Chem. 277*, 48643−48649.
20. D'Alessio, G., Di Donato, A., Parente, A., and Piccoli, R. (1991) *Trends Biochem. Sci. 16*, 104−106.
21. D'Alessio, G., Malorni, M. C., and Parente, A. (1975) *Biochemistry 14*, 1116−1122.
22. Smith, G. K., and Schaffer, S. W. (1979) *Arch. Biochem. Biophys. 196*, 102−108.
23. D'Ursi, A., Oschkinat, H., Cieslar, C., Picone, D., D'Alessio, G., Amodeo, P., and Temussi, P. A. (1995) *Eur. J. Biochem. 229*, 494−502.
24. Crescenzi, O., Carotenuto, A., D'Ursi, A. M., Tancredi, T., D'Alessio, G., Avitabile, F., and Picone, D. (2001) *J. Biomol. NMR 20*, 289−290.
25. Sica, F., Di Fiore, A., Zagari, A., and Mazzarella, L. (2003) *Proteins*, in press.
26. Di Donato, A., and D'Alessio, G. (1981) *Biochemistry 20*, 7232−7237.
27. Kunitz, M. (1946) *J. Biol. Chem. 164*, 563−568.
28. Parente, A., Albanesi, D., Garzillo, A. M., and D'Alessio, G. (1977) *Ital. J. Biochem. 26*, 451−466.
29. Delaglio, F., Grzesiek, S., Vuister, G., Zhu, G., Pfeifer, J., and Bax, A. (1995) *J. Biomol. NMR 6*, 277−293.
30. Johnson, B. A., and Blevins, R. A. (1994) *J. Biomol. NMR 4*, 603−614.
31. Wishart, D. S., Bigam, C. G., Yao, J., Albigaard, F., Dyson, H. J., Oldfield, E., Markley, J. L., and Sykes, B. D. (1995) *J. Biomol. NMR 6*, 135−140.
32. Zuiderweg, E. R. P., and Fesik, S. W. (1989) *Biochemistry 28*, 2387−2391.
33. Marion, D., Kay, L. E., Sparks, S. W., Torchia, D. A., and Bax, A. (1989) *J. Am. Chem. Soc. 111*, 1515−1517.
34. Vuister, G. W., and Bax, A. (1993) *J. Am. Chem. Soc. 115*, 7772−7777.
35. Archer, S. J., Icura, M., Torchia, D. A., and Bax, A. (1991) *J. Magn. Reson. 95*, 636−641.
36. Bax, A., Icura, M., Kay, L. E., Torchia, D. A., and Tschudin, R. (1990) *J. Magn. Reson. 86*, 304−318.
37. Farrow, N. A., Muhandiram, R., Singer, A. U., Pascal, S. M., Kay, C. M., Gish, G., Shoelson, S. E., Pawson, T., Forman-Kay, J. D., and Kay, L. E. (1994) *Biochemistry 33*, 5984−6003.
38. Santoro, J., Gonzales, C., Bruix, M., Neira, J. L., Nieto, J. L., and Rico, M. (1993) *J. Mol. Biol. 229*, 722−734.
39. Neira, J. L., Sevilla, P., Medendez, M., Bruix, M., and Rico, M. (1999) *J. Mol. Biol. 285*, 627−643.
40. Capasso, S., Giordano, F., Mattia, C. A., Mazzarella, L., and Zagari, A. (1983) *Biopolymers 22*, 327−332.
41. Güntert, P., Mumenthaler, C., and Wüthrich, K. (1997) *J. Mol. Biol. 273*, 283−298.
42. Güntert, P., Braun, W., and Wüthrich, K. (1991) *J. Mol. Biol. 217*, 517−530.
43. Güntert, P., Braun, W., Billeter, M., and Wüthrich, K. (1989) *J. Am. Chem. Soc. 111*, 3997−4004.
44. Baker, W. R., and Kintanar, A. (1996) *Arch. Biochem. Biophys. 327*, 189−199.
45. Pearlman, D. A., Case, D. A., Caldwell, J. W., Ross, W. S., Cheatham, T. E., III, DeBolt, S., Ferguson, D., Seibel, G., and Kollman, P. A. (1995) *Comput. Phys. Commun. 91*, 1−41.
46. Weiner, S. J., Kollman, P. A., Nguyen, D. T., and Case, D. A. (1986) *J. Comput. Chem. 7*, 230−238.

47. Baxter, N. J., and Williamson, M. P. (1997) *J. Biomol. NMR 9*, 359−369.
48. Koradi, R., Billeter, M., and Wüthrich, K. (1996) *J. Mol. Graphics 14*, 51−55.
49. Kraulis, P. J. (1991) *J. Appl. Crystallogr. 24*, 946−950.
50. Price, W. S. (1997) *Concepts Magn. Reson. 9*, 299−336.
51. Price, W. S. (1998) *Concepts Magn. Reson. 10*, 197−237.
52. Wu, D., Chen, A., and Johnson, C. S., Jr. (1995) *J. Magn. Reson., Ser. A 115*, 260−264.
53. Laskowski, R. A., Rullmannn, J. A., MacArthur, M. W., Kaptein, R., and Thornton, J. M. (1996) *J. Biomol. NMR 8*, 477−486.
54. Ramachandran, G. N., and Sasisekharan, V. (1968) *Adv. Protein Chem. 23*, 283−437.
55. Shimotakahara, S., Rios, C. B., Laity, J. H., Zimmerman, D. E., Scheraga, H. A., and Montelione, G. T. (1997) *Biochemistry 36*, 6915−6929.
56. Di Donato, A., Cafaro, V., and D'Alessio G. (1994) *J. Biol. Chem. 269*, 17394−17396.
57. Cole, R., and Loria, J. P. (2002) *Biochemistry 41*, 6072−6081.

BI0342517